Classification:
Biological Sciences: Biophysics.

Common Mechanism of Pore Opening Shared by Five Different Potassium Channels

Indira H Shrivastava and Ivet Bahar

Department of Computational Biology, School of Medicine, University of Pittsburgh, Pittsburgh, PA 15213, USA

Corresponding Author:
Ivet Bahar

Manuscript Information:
10 pages, including references, figure legends,

Word and character counts:
Abstract: 199 words, 1376 characters, including spaces
Text: 9145 words, 58,196 characters, including spaces (including figure captions, tables, references).

Abbreviations:
TM: transmembrane; EC: extracellular; CP: cytoplasmic; GNM: Gaussian Network Model; NMA: normal mode analysis; ANM: anisotropic network model; ENM: elastic network model

Abstract

A fundamental question associated with the function of ion channels is the conformational changes that allow for reversibly opening/occluding the pore through which the cations permeate. The recently elucidated crystal structures of potassium channels reveal similar structural motifs at their pore-forming regions, suggesting that they share a common gating mechanism. The validity of this hypothesis is explored by analyzing the collective dynamics of five known K^+ channel structures. Normal mode analysis using Gaussian Network Model (GNM) strikingly reveals that all five structures display the same intrinsic motions at their pore-forming region despite the differences in their sequences, structures and activation mechanisms. Superposition of the most cooperative mode profiles shows that the identified common mechanism is a global cork-screw like counter-rotation of extracellular (EC) and the cytoplasmic (CP) regions, leading to the opening of the CP end of the pore. A second cooperative mode shared by all five K^+ channels is the extension of the EC and/or CP ends via alternating anticorrelated fluctuations of pairs of diagonally opposite monomers. Residues acting as hinges/anchors in both modes are highly conserved across the members of the family of K^+ channel proteins, consistent with their presently disclosed critical mechanical role in pore gating.

Introduction

The functions of ion channels include establishing a resting membrane potential, controlling cell volume and regulating flow of ions across epithelial cells (1). Diseases caused by mutations in ion channels, termed as channelopathies, potentially impair cell-cell communication and lead to neurodegenerative disorders or muscular diseases such as multiple sclerosis (2). The molecular conformational mechanisms underlying the (dys)function of ion channels remain, however, elusive.

Membrane proteins are typically composed of three domains: extracellular (EC) domain exposed to the periplasm, intracellular/cytoplasmic (CP) domain buried in the cytoplasm, and the transmembrane (TM) domain embedded in the lipid bilayer. The TM domain is composed of a bundle of helices contributed by four identical monomers in potassium (K^+) channels, which encloses a pore, or a channel, through which ions are conducted. The pore regions of most K^+ channels are considered to have similar structural characteristics: a narrow selectivity filter at the EC side, followed by a large cavity in the middle and ending in a long gating region that connects to the CP region.

Potassium channels are ~10^4 times more selective to K^+ ions than to Na^+ ions (3). This propensity for K^+ is attributed to the selectivity filter residues (GYG) also known as the 'signature sequence' conserved in both eukaryotic and prokaryotic K^+ channels (3). One of the fundamental questions associated with the gating of K^+ channels is the location of the activation gate and the molecular conformational changes that ensure a reversible opening/occlusion of the pore.

The bacterial K^+ channel from *Streptomyces lividans* (KcsA) is the first K^+ channels crystallized and structurally determined (3). Since then, several more K^+ channel structures have been determined, all tetramers like KcsA, albeit in different conformations and with different structural topologies, including Mthk (4), KirBac 1.1 (5), KvAP (6) and Shaker (7). The crystal structures of MthK and KvAP are considered to be in the 'open' form, while those of KcsA and KirBac are 'closed'. The organisms, resolutions and Protein Data Bank (PDB) (8) identifiers associated with these five structures are listed in Table 1, along with the size of their monomers and the residue numbers corresponding to the signature sequence GYG in each case.

Sequence alignment of these five structurally known K^+ channels reveals 18%-28% sequence similarity with KcsA in the pore forming domain (Figure 1a). The pore regions also share a common structural topology (Fig. 1b), mainly four pairs of transmembrane (TM) helices contributed by each monomer, denoted as TM1 (outer, yellow) and TM2 (inner, green) helices, connected by the P-loop region (red) on each monomer. The P-loop regions consist each of a short P-

helix, the selectivity filter and the turret (Fig 2). Gating is activated by different factors in these K^+ channels: KcsA is gated by pH change (3), MthK by intracellular Ca^{2+} binding (4), KirBac by phosphatidylinositol 4,5-bisphosphate (PIP_2) modulation (9) and ATP binding at the cytoplasmic β-domains (5), KvAP (6) and Shaker (7) by voltage-difference across the membrane. Kirbac and MthK have an additional CP domain attached to their TM domain. Their monomers contain two TM helices each, like KcsA. KvAP (6) and Shaker(7), on the other hand, contain six TM helices: they are known as 6TM structures, although their pore-forming region is structurally similar to that of KcsA (Fig. 1b). The structural similarity at the pore region suggests a similar gating mechanism shared by all K^+ channels although the validity of this hypothesis needs to be tested. More importantly, the conformational motions that underlie the gating of the pore for K^+ conduction remain to be elucidated. The present study aims at answering these fundamental questions.

Several experimental studies have been carried out to date, to elucidate the conformational changes associated with pore opening in K^+ channels (9-14). Prominent among these are the studies by Perozo and coworkers (13,14) where the molecular events associated with the activation of KcsA were investigated by site-directed spin-labeling and electron paramagnetic resonance (EPR) spectroscopy. Based on their results, Perozo and coworkers suggested that the M2 helices rotate in a counterclockwise direction when viewed from the EC side, while swinging away from the permeation pathway, thus increasing the diameter of the pore cavity (13). This motion was pointed out to be accompanied by that (counterclockwise rotation) of the M1 helices. These experiments also indicated the intrinsic rigidity of the selectivity filter as compared to the flexibility of the M2 helices, particularly towards the CP side.

While these structural and spectroscopic studies provide insightful details on the channel pore interactions, the precise conformational changes that accompany the opening/closing of the channel during gating and their molecular basis, remain elusive. The increasing experimental data on K^+ channel structures now provides a foundation for structure-based computational studies. The availability of the atomic coordinates of KcsA has indeed generated a plethora of computational studies (15-27) and with the additional K^+ channel structures elucidated in the last two years, a comparative analysis of cooperative motions near the pore region can potentially provide new insights, which is the focus of the present study.

The conventional computational approach for exploring the dynamics of KcsA has been to perform molecular dynamics (MD) simulations at atomic scale with explicit solvent and lipid molecules. Due to the large size of the system (typically > 50K atoms) the generated trajectories are typically restricted to short times, of the order of nanoseconds. As such, MD simulations, including our previous work (15,16,20,26), have been unable to elucidate the collective structural changes

involved in channel gating, which are at least 1-2 orders of magnitude slower. Many targeted or steered MD simulations have been resorted to, in order to accelerate the simulations and explore the functional motions of K^+ channels. In particular, the closed and open structures of KcsA and MthK, respectively, have been used as end points to model the gating mechanism (23,24). Biggin and Sansom simulated the opening of KcsA by gradually increasing the volume of a particle at the putative CP gate region (23).Tikhonov and Zhorov applied lateral forces on the inner ends of the M2 helices (see below) to open up the pore (24). There have been examples of notable successes in predicting the KcsA ion binding sites (25,26) and in estimating the free energy profile that facilitates ion permeation through the selectivity filter (27). Yet, the large scale motions that cooperatively engage the entire molecule, and in particular those instrumental in gating, remained beyond the reach of MD simulations in general.

Another computational approach that has found wide applications in recent years for exploring long-time/ large scale dynamics is normal mode analysis (NMA) with coarse-grained models. NMA has been applied to proteins since the early 80s (28-30), but its utility as an efficient approach for a first assessment of functional motions has been fully recognized only recently, after verifying in many applications the strong correlation between the most cooperative (usually the lowest frequency, also called *global*) modes of motions predicted by NMA and the functional motions inferred from experiments (31-33). A recent NMA by Ma and coworkers already demonstrated its utility for providing insights into the gating mechanism of KcsA (34). Given the insensitivity of global modes to detailed atomic interactions (35), reduced models (e.g. elastic network models - ENMs) have been adopted for identifying such *intrinsic* dynamics, starting from the Gaussian Network Model (GNM) (36,37) built on statistical mechanical theories introduced for polymer networks (38), which led the way to a wealth of applications and extensions (32,33,39-52).

In the present work, the equilibrium dynamics of KcsA, KirBac, MthK, KvAP and Shaker (see Fig 1) are analyzed using ENMs. We focus on the slowest non-zero modes predicted by the GNM and the anisotropic model (ANM) (41), and demonstrate that all five K^+ channels possess the same type of intrinsic global dynamics for regulating the pore opening/closing at the putative intracellular gate. The most cooperative mechanism of conformational change invariably predicted for all five structures is *a global torsion*, manifested by the counter-rotations of the EC and CP regions around the cylindrical axis, similar to a cork-screw mechanism, and simultaneously inducing an enlargement of the pore at the CP end. The second most cooperative mode is an alternating expansion/contraction of EC and/or CP ends via anticorrelated fluctuations of oppositely located pairs of monomers. This type of motion is likely to facilitate the binding and access of toxins to the central constriction zone. The results are shown to explain and complement the experimental observations of Perozo and

coworkers (13,14) and permit us to identify the key sites/residues that control the functional mechanics of the potassium channels.

Material and Methods

GNM. Detailed description of the GNM can be found in the literature (33, 35). We discuss here only the salient features, only, of the model.

The structure is represented by a network of *N* nodes identified by the α-carbons. The pairs of nodes within a cutoff distance R_c of 7.0 Å are assumed to be connected by uniform springs of force constant γ, representative of the interactions that stabilize the native fold. The inter-residue contact topology is fully defined by the NxN Kirchhoff matrix, the elements of which are defined as

$$\Gamma_{ij} = \begin{cases} -1 & i \neq j \text{ and } R_{ij} \leq R_c \\ 0 & i \neq j \text{ and } R_{ij} > R_c \\ -\sum_j \Gamma_{ij} & i = j \end{cases} \quad (1)$$

The inverse of Γ provides information on the mean-square (ms) fluctuations $\langle(\Delta R_i)^2\rangle$ of residues (diagonal elements) and their cross-correlations (off-diagonal elements), similarly to the inverse of the Hessian in NMA, i.e.

$$\langle(\Delta R_i)^2\rangle = (3k_BT/\gamma)[\Gamma^{-1}]_{ii} \quad (2)$$

where *T* is the temperature and k_B the Boltzmann constant.

Global modes of motion. A major utility of the GNM is the decomposition of the fluctuation spectrum into a set of normal modes, or the extraction of the slow (or global) modes with minimal computational cost. The contribution of the k^{th} nonzero mode ($1 \leq k \leq N-1$) to $\langle(\Delta R_i)^2\rangle$ is given by (36)

$$[(\Delta R_i)^2]_k = (3k_BT/\gamma)\ \lambda_K^{-1}\ [\mathbf{u}_K]_i^2 \quad (3)$$

where $\mathbf{u}_k$ and λ_k are the respective k^{th} eigenvector and eigenvalue of Γ. λ_k scales with the frequency of mode *k*, and the i^{th} element of $\mathbf{u}_k$, $[\mathbf{u}_K]_i$, provides a measure of the displacement of residue *i* along the k^{th} mode coordinate. In particular $[\mathbf{u}_1]_i$ reflects the mobility of residue *i* in the *1st (slowest)* mode (note that $\lambda_0 = 0$). Its distribution as a function of residue index *i* is termed the *global mode shape*.

The slow modes usually have high collectivity (51). Several studies have shown that a small subset of slow modes are usually implicated in molecular motions relevant to biological function (31-33,39-49,51-53). The most constrained (or the least mobile) residues in these modes play a key mechanical role such as acting as hinge centers or regulating the concerted movements of entire domains. A

major utility of the GNM is indeed the identification of such *mechanically critical sites*.

Anisotropic network model (ANM). The GNM provides information on the *magnitude* of fluctuations, not on their *directions,* and these fluctuations are isotropic by definition, i.e. $\langle(\Delta X)_i^2\rangle = \langle(\Delta Y)_i^2\rangle = \langle(\Delta Z)_i^2\rangle = \langle(\Delta R)_i^2\rangle/3$. To characterize the directions of motions, we adopt the ANM (41). Γ is replaced therein by the *3Nx3N* Hessian matrix $\boldsymbol{H}$, the elements of which are found from the 2nd derivatives of the ANM potential

$$V_{ANM} = (\gamma/2) \sum_i \sum_{j>i} \Gamma_{ij} (R_{ij} - R_{ij}^0)^2 \qquad (4)$$

with respect to α-carbon positions. Note that the ANM potential differs from the one implicitly assumed in the GNM,

$$V_{GNM} = (\gamma/2) \sum_i \sum_{j>i} \Gamma_{ij} (\boldsymbol{R}_{ij} - \boldsymbol{R}_{ij}^0) \cdot (\boldsymbol{R}_{ij} - \boldsymbol{R}_{ij}^0) \qquad (5)$$

in that V_{ANM} depends on the *magnitudes* of the initial (R_{ij}^0) and final (R_{ij}) inter-residue distances, not penalizing the changes in *orientation* that maintain the inter-residue distances, while V_{GNM} depends on the vectorial difference, i.e. GNM takes account of internal orientational deformations in addition to distance changes. In this respect, the ANM is less realistic than the GNM, but it has the advantage of yielding information, albeit approximate, on the components of $\Delta\boldsymbol{R}_i$.

Generation of accessible and potentially functional reconfigurations. Conformational changes favored by a given mode *k* can be assessed using the ANM-predicted eigenvector $\boldsymbol{u}_k^{ANM}$ in

$$[\boldsymbol{R}(\pm s)]_k = \boldsymbol{R}^0 \pm s_k \lambda_k^{(-½)} \boldsymbol{u}_k^{ANM} \qquad (6)$$

Here, $\boldsymbol{R}^0$ and $\boldsymbol{R}$ represent the *3N*-dimensional vectors of the original and instantaneous positions, respectively, of all amino acids, the subscript *k* refers to the mode that induces the conformational change, and s_k is a parameter uniformly scaling the size of the deformation induced by mode *k* (52).

Structural details on the 2TM pore. Most K^+ channels are homotetrameric and four-fold symmetric around the pore (cylindrical, z-) axis. The pore is surrounded by four pairs of TM helices, called TM1 and TM2 in KcsA. As illustrated for KcsA (Fig. 2a), the outer helices (TM1) are exposed to the hydrophobic lipid environment while the inner helices (TM2) face the pore. The entire length of the pore is ~34 Å. The P-loop is comprised of the selectivity filter, the P-helix, which spans only the upper half of the bilayer, and the exposed loops, known as the turret (3). The four P-loops together form the EC vestibule, enclosing a narrow selectivity filter region ~10 Å in length, which opens up into a large

central cavity of ~10 Å in diameter. This central cavity is connected to the cytoplasm by a hydrophobic pore ~18 Å in length, containing the putative gate region. The pore forming regions of MthK, KirBac, KvAP and Shaker have topology similar to that of KcsA (Fig. 1b).

As pointed out above, the selectivity filter residues GYG (Table 1) play a critical role in selecting K^+ over Na^+ for permeation (3). The examined K^+ channels also contain another conserved glycine on the TM2 helices (Fig. 1a, magenta box): G^{99}(KcsA), G^{83}(MthK), G^{134}(KirBac), G^{220}(KvAP) and G^{398}(Shaker). G^{99} is considered to play an important role in KcsA tetramerization (56). Finally, in the MthK structure, which is in the open state, there is a kink observed at G^{83} on TM2, which is considered to play a role of 'gating hinge' in pore opening (22).

MD simulations. MD simulations of KcsA (1k4c) were carried out in a lipid-bilayer solvated with explicit water molecules and three potassium ions in the selectivity-filter and the cavity using GROMACS (53). An equilibration run of 300 ps was performed first, during which the protein backbone atoms were restrained by a harmonic potential, and the lipid (phosphatidylethanolamine) (POPE) and water molecules were allowed to relax. This was followed by a production run of 7ns during which the position constraints on the protein were removed.

Results and Discussions

Equilibrium fluctuations. Before proceeding to the characterization of the global modes of motions, it is of interest to assess the applicability of the GNM in so far as the equilibrium dynamics of the ion channels is concerned. To this aim, we compared the distributions of residue fluctuations predicted for KcsA by the GNM with (i) experimental data (X-ray crystallographic B-factors), and (ii) results from full atomic MD simulations. The experimental B-factors $B_i = 8\pi^2 <(\Delta R_i)^2> /3$ are taken from the PDB file 1k4c (54) (Table 1); and the fluctuations from MD simulations are computed from trajectories of 7 ns with explicit solvent and lipid molecules, using the averages over 140 snapshots taken at 50 ps intervals.

Figure 2 panel b compares the B-factors (left ordinate) or corresponding ms fluctuations (right ordinate) obtained for KcsA from GNM analysis (red curve), MD simulations (black) and X-ray crystallographic measurements (blue). The GNM curve is obtained using eq 2, with γ = 4.82 kcal/mol Å^2. Note that the absolute value of γ does not affect the profile, but uniformly rescales all fluctuations.

The correlation coefficients between the results for the respective pairs GNM/MD, GNM/X-ray and MD/X-ray are 0.93, 0.94, and 0.83. The GNM results indeed exhibit an even better agreement with experimental data than that exhibited by

MD simulations. The higher performance of GNM deserves attention given that this occurs despite the facts that (i) the GNM is a coarse-grained model that does not include any specific interaction at the atomic scale, while these are included in MD force fields and simulations, and (ii) the experimental data may also contain biases/errors due to static disorder or intermolecular contacts. One explanation is that the GNM results, being a *unique analytical* solution for the given structure, are devoid of any sampling inaccuracy that MD simulations may incur. One may indeed notice that the GNM yields identical results across all four monomers in accord with the four-fold symmetry of the structure, while the MD simulations yield different fluctuation behavior for the monomers due to random/incomplete sampling. A second explanation is the fact that GNM contains contributions, albeit approximate, from the *complete* spectrum of equilibrium modes, including in particular the slowest modes that involve the entire structure, which cannot be sampled within the 7 ns MD simulations.

The above analysis supports the utility and accuracy of the GNM in so far as the equilibrium fluctuations are concerned, but does not provide any information different from that already observed by experiments. We now proceed to the spectral decomposition of GNM dynamics to gain insights into the underlying dominant/cooperative modes that are potentially relevant to biological function.

Cooperative/global motions. Two mechanisms of global motions have been identified for all five examined structures, referred hereafter as motions of type I and II, respectively. The motion of type I is doubly degenerate, i.e. it results from the combination of two symmetrically related modes with identical frequency; type II motion is non-degenerate. While both the modes are proposed to be functional, the second (type II) directly ensures pore opening, as will be described below.

Distribution of residue displacements driven by global modes. Figure 3 presents an overview of the shapes of the global modes of type I (left panels) and both types (right panel) for the tetramer (left) or a monomer (right). The curves are the normalized distributions (of profiles) of residue mobilities (square displacements) induced by the particular modes (see eq 3). The left panels exhibit the four-fold symmetry of the motions consistent with the homotetrameric structures.

Two important observations are made with regard to the shape of the modes in Figure 3. The minima in global mode of type I precisely coincide with the signature motif GYG (Table 1) of the ion *channels in all five cases*. The minima in global mode profiles have been shown in several studies to point to the *mechanically critical sites* of the examined structures (32, 33). Strikingly, here the selectivity filter, and in particular the signature sequence GYG, emerges as the most severely constrained element of the structure in all five structures. The position of the GYG motif is indicated by the ‘x’ signs along the abscissa.

The selectivity filter residues are distinguished by their low mobilities not only in the motion of type I, but also in type II motions, as can be inferred from the minima in the red curves on the right panels. It is noteworthy to mention that our MD simulations of KcsA in an explicit solvent-bilayer environment (15) also revealed negligibly small fluctuations at the selectivity filter region. The high stability of the selectivity filter backbone is presumably a biological requirement for precise functioning (selective conduction) of K^+ channels.

The second observation of interest relates to the minima in the modes of type II. These positions indicated by the red '●' signs on the right panels in Figure 3 refer to centrally located residues in the TM1 and TM2 helices. The minima on TM2 helices are located at, or in the close vicinity of, the conserved Gly mentioned above, mainly at G^{99}(KcsA), G^{83}(MthK), G^{134}(KirBac), A^{223}(KvAP) and Shaker(L^{400}). The occurrence of a gylcine at a slow mode minimum suggests that this residue may serve as a 'hinge' site for a global motion. Furthermore, the conservation of these glycines across all five ion channels (Figure 1a) suggests a conserved mechanism of motion (4). The minima on the TM1 helices (shown by the symbol '▲' along the abscissa), on the other hand, occur at small hydrophobic residues - V^{37}(KcsA), I^{32}(MthK), V^{73}(KirBac), A^{156}(KvAP) and L^{335} (Shaker), that are spatially close to the conserved Gly on TM2. The small size of these residues allows for close van der Waals interactions and rotational flexibilities. These results suggest that these TM1 residues are possibly implicated, along with the conserved Gly on TM2 helices, in a pivotal role in the global motion of type II.

Visualization of mobilities. A better assessment of mobilities is possible by mapping the results in Figure 3 into color-coded ribbon diagrams. Figure 4 illustrates the results for KcsA, KirBac and Shaker. The colors range from red (most mobile) to blue (static). The panels on the left two columns illustrate the results for *each* of the doubly degenerate modes of type I, and those on the right column refer to mode type II.

The pairs of diagonally opposite monomers exhibit identical fluctuation behavior in mode type I (Figure 4 left column), and the roles of the pairs are inverted in the accompanying 2^{nd} degenerate mode (middle column). As will be shown below, in type I motion, a given pair of oppositely positioned TM1 helices move away from the pore region, giving rise to *a distortion from circular symmetry into an ellipse* when viewing the cross-sectional area while the other pair is stable, and vice versa. The motions are enhanced towards the EC region and peak at the turrets in KcsA, while a higher mobility towards the CP region is observed in KirBac (and MthK, not shown). Shaker (and KvAP, not shown) exhibit high mobilities at both ends. The cross-correlations and ANM results below show that the diagonally positioned pairs of monomers are subject to anticorrelated (i.e. concerted, but opposite sense) fluctuations, allowing for the opening of the EC and/or CP ends via concerted, alternating movements of the pairs of monomers.

Motion of type II, on the other hand, emerges as a very robust mode, identically recruited by all five structures. The four monomers undergo the same fluctuation behavior in this mode, i.e. the motion is four-fold (or cylindrically) symmetric. This motion amplified towards the CP end of the ion channels will be shown below to be a *global torsion* that controls the gating of the pore.

The most cooperative (lowest frequency) modes computed here therefore reveal that despite their sequence, structure and activation mechanism dissimilarities, all five potassium channels bear close resemblance in so far as their global motions are concerned, and it will be shown below that *the global mode of type II is directly involved in pore gating.*

Master curves for all five K^+ channels global dynamics. While the mode shapes Figure 3 appear to be somewhat different, their superimposition after correcting for the residue insertions/deletions indicated by their sequence alignment (Fig. 1a) leads to the master behavior of all ion channels displayed in Figure 5. Panels a and b refer to the global modes of types I and II, respectively. The residue numbers of MthK are used as reference along the abscissa.

Major features in these master curves are summarized as follows.

In so far as the collective motions of type I (Fig 5a) are concerned;

- all five structures exhibit a definite preference for severely constraining the signature motif GYG as a global minimum, irrespective of the differences in the mobilities of the other regions,
- KcsA is distinguished by the peaks near the turrets and lower mobility towards both N- and C-termini, while all others exhibit increased mobilities towards their N- termini (at the CP region),
- the C-terminus (i.e. CP ends of TM2 helices), on the other hand, shows a mixed behavior. KcsA, KirBac and KvAP are stable at this region, while MthK and Shaker show increased mobilities.

In so far as the collective motions of type II (Fig 5b) are concerned,

- all five chains again exhibit a high stability at the selectivity filter region
- a minimum is observed at a central position in both the TM1 and TM2 helices in all five structures, revealing a change in the direction of collective motion at a central plane. This inversion will be shown below to refer to a cross-sectional plane almost bisecting the TM helices.
- the minima on the TM2 helices exactly coincide with, or closely neighbor, the conserved Gly residues pointed out in previous experiments to be functionally important in KcsA (G^{99}) (13) or form a kink (e.g. G^{83} in MthK (4)). Those on TM1 helices, on the other hand, occupy a position spatially close to these kink sites, suggesting a possible bending of *all* helices, in addition to global inversion of rotation direction, at the same central plane.

As will be shown below, the global motion of type II is mainly responsible for gating the pore. Indeed this combination of global torsion with outward bending of the TM1 and TM2 helices' cytoplasmic halves that will ensure the cooperative pore opening, consistent with experimental observations.

Mechanisms of global motions and relevance to gating. The mechanisms of the global motions of type I and II are elucidated by ANM analysis.

We first focus on KcsA. The strategy is as follows: we identify the ANM modes that are equivalent to the above determined GNM modes of types I and II, by comparing the eigenvectors derived from $\boldsymbol{\Gamma}$ and $\boldsymbol{H}$, and sorting pairs that yield most correlated square displacements. ANM thus permits us to compute the X-. Y- and Z- components of the fluctuations driven by the global motions of type I and II, or the deformation vectors, which upon substitution in eq 6 permit us to generate the 'deformed' states, or the alternative conformations sampled by the actions of modes I and II. These alternative states are consistent with the notion of the native (macro)state as an ensemble of microstates defined by the normal fluctuations in the neighborhood of the known structure.

Figure 6 illustrates the alternative conformations sampled by KcsA near its original (PDB) structure. Two different pathways of reconfiguration are shown, referring to global modes of type I and II. Panel a displays the side views of the native state and two conformations favored by the mechanisms I and II. Panel b displays the top views of the same structures. The central structure is the original structure, and the four alternative forms are those sampled by mechanisms I and II, again, but this time we display both the positive and negative departures away from the original state by adopting the scaling parameters of $\pm s_I = 75$ or $\pm s_{II} = 100$ for visualizing the respective modes (see eq 6). This parameter scales the *size* of the motion without affecting its *mechanism*.

We note that positive and negative fluctuations are equally probable, by definition, in the immediate neighborhood of the global energy minimum in NMA. Larger scale deformations may entail a preference in one direction or another due to the anharmonicity of the energy landscape. The present study sheds light to the initial events, only, in the close neighborhood of the native state.

The emerging mechanisms of motions are as follows:

Motion of type I involves the concerted anticorrelated opening/closing of the EC ends of the diagonally positioned pairs of monomers. As a given pair of monomers move away from each other, the opposite pair come close, such that the cross-sectional area viewed from the top oscillates between a circular (native) and elliptic (deformed) shape, the long axis of the ellipse alternating between the two perpendicular directions depending on the 'stretched' monomers. The pore

region remains practically fixed during this motion, while the EC ends of the molecule, and in particular the turrets undergo large swinging motions.

Motion of type II is a global torsion. During this cooperative motion, the EC regions of the molecule rotate counter-clockwise, while the CP domains rotate clockwise, and vice versa. The amplitude of the motion becomes larger with increasing distance from a stationary plane that comprises the central parts of TM1 and TM2 helices. As pointed out above, this central plane includes the conserved glycines on TM2 and a set of small hydrophobic residues of TM1 helices that form a stable core. The amplification of the motion away from this plane is particularly pronounced towards the CP ends of TM2 helices, and confers a remarkable expansion and mobility at the intracellular gate region, while the selectivity filter remains fairly rigid. The pore enlargement is induced by the rotations in either direction, as can be discerned in panel b. This structure-induced ability of KcsA to open the pore via concerted tilting and rotation of the TM1 and TM2 helices was also pointed out by Ma and coworkers (34) in their insightful NMA of KcsA intrinsic dynamics. Interestingly, the same mechanisms of motions are observed here not only for KcsA, but across all five potassium channels structurally characterized to date. The counterpart of Figure 6b for Shaker is given in Figure 6c.

Pore enlargement induced by mode II: **A closer view of constriction zone.** The expansion of the pore region induced by mode II can be directly viewed by plotting the radius of the central constriction zone as a function of the position along the z-axis. The black curve in Figure 7 displays the profile for the original (KcsA) structure. As illustrated in panel b, the selectivity filter region is the region with the lowest (~1 Å) radius, shown in red, succeeded by the pore region of 1.5-2 Å radius (green). The central cavity enjoys significant radial enlargement (up to 4.5 Å, blue region), as well as the EC end of the molecule. The fluctuating conformations induced by the action of mode II, on the other hand, lead to the solid and dotted curves shown in red in panel a, which refer to the respective global torsions in opposite directions (positive and negative deformations induced by using $\pm s_{II}$). The selectivity filter remains practically unchanged during this reconfiguration, while there is a significant increase in the internal radius at the position of the intracellular gate. The pore region diameter widens up to 7 Å using $\pm s_{II} = 100$. This behavior is illustrated by the lower diagram, where the expansion in the pore region can be visualized. The inset in panel a also displays the relative position of the CP ends of the TM2 helices (blue/red before/after global torsion). For simplicity two opposite monomers are displayed here. Interestingly, this diagram shows close resemblance to that obtained by the superposition of the crystal structures of KcsA and MthK (4), supporting the view that the deformed state presently predicted is the open form of KcsA.

Calculations repeated for the four other K^+ channels showed that the global torsion cooperatively modulating the opening of the pore is commonly shared by

all potassium channels. See the movies (supplementary data 1-4) for an animated visualization of the conformational fluctuations associated with mode II for KcsA and Shaker.

Comparison with Experimental Data. Most K^+ channels are known to be blocked by large organic cations such as tetrabutyl ammonium (TBA) from CP side and tetraethylammonium (TEA) from both sides of the membrane (3). The size of these cations is ~7-12 Å. The fact that these molecules can enter the pore and bind at the CP end of the selectivity filter, suggests that the gate must be opening up very wide, in order to accommodate the cation. The crystal structure of MthK (4) also supports this argument, since in the crystal structure, the TM2 helices are bent away from the pore axis, increasing the diameter of the pore to greater than 12 Å. The top diagrams in panels A and B of Figure 8 illustrate the experimentally proposed mechanisms for KcsA and MthK gating, respectively (13,14). Such large conformational changes are also indicated in mutational studies done on Shaker (55). These studies in fact, propose a similar opening mechanism for both the voltage-gated and voltage-independent K^+ channels. The torsional motion seen here in most cooperative global mode, for all the proteins, irrespective of the gating ligand, supports the common gating mechanism view.

In Fig. 8a, the opening of the KcsA pore from the closed form to the 'open' form predicted by GNM (shown by the green diagrams) is clearly seen, to be in accord with that proposed by models based on experimental data (13) and crystal structures (14). The diagrams illustrate the relative positions of the four TM2 helices, prior to deformation ($s_{II} = 0$), or as induced by mode II ($s_{II} \neq 0$). Similar results are presented for Shaker and Kirbac (last row in both panels). In Shaker, since the pore is already open, this mode pushes the intracellular region of TM2 (beyond the Gly 'kink') outwards and away from the pore axis.

A striking observation is the appearance of a kink, in addition to an overall enlargement, with increase in the extent of deformation. The kink occurs at T^{107} in KcsA, and at the conserved G^{134} in KirBac1.1 (Fig. 8B), at $s_{II} = 150$ and 73 respectively. The residue T^{107} which is a minima in type I mode in KcsA, was also found to provide a binding site to the ion in the cavity in MD simulations (15); and in the NMA of KcsA (34), the residues T^{107}-L^{110} were considered to be at a pivotal position in the gating mechanism. Notably, two mutants, A108S and A108T have been observed (56) to dramatically increase the population of open KcsA conformers, consistent with the critical importance of this region for mediating pore opening. In addition, mutation of T107 in KcsA resulted in dramatic reduction in current (57). The 'kink' formation presently predicted at this conserved residue is in accord with the hypothesis (4) that the region at or around the conserved Gly serves as a 'hinge' in the gating mechanism. It should be noted here that the kink in TM2 forms after the pore opens up, not before that. Compare for example the results for KcsA for different extents of deformation (Fig. 8a).

Finally, we note that in Shaker, the minima in the type II mode is at L400, which is in close proximity to the 'PVP' motif conserved in Kv channels. Cross-linking studies suggest that a distortion may occur at TM2 in Shaker (known as S6 in Kv channels) in the vicinity of the PVP motif (58-59), which lends further support to the physical realism of the predicted motions.

Conclusion

The process of channel opening requires structural rearrangement of the ion conduction pathway. The channels show narrow constrictions within the pore, which maybe broadening and contracting as the channel gates. Such cooperative conformational changes, though anticipated by experimental results, have never been accessed so far, either by intensive MD simulations of KcsA equilibrium dynamics or even non-equilibrium simulations, except for the NMA conducted by Ma and coworkers (34). A simple analytical model purely based on contact topology/geometry has provided here a scaffold for the conformational changes involved not only at the putative intracellular gate but also at the EC turret region of KcsA. Most importantly, a common pore gating mechanism is revealed by the present analysis for all five structurally determined potassium channels. While these K^+ channels differ in their sequences (Figure 1a), structures (Figure 1b) and activation mechanisms, by focusing on their pore-forming region, and optimally aligning their sequence, master curves for two dominant mode shapes shared by all five channels emerged, presented in Figure 5.

Mode I is shown to be manifested by anticorrelated fluctuations of oppositely located monomers, to deform the cylindrical symmetry of the structure and expose the CP and/or EC regions to facilitate ligand/toxin binding from either end.

Mode II, on the other hand, which is proposed here to be the major mechanism involved in channel gating, is a global torsion, i.e. counter-rotation of the two halves of the molecule, simultaneously inducing a substantial broadening in the pore region. This mode further gives rise to the formation of a kink at a conserved glycine in all K^+ channels, after a certain level of enlargement of the pore region.

While the TM helices and CP/EC domains undergo significant rearrangements in these global modes, the selectivity filter remains highly stable (see the minimum at the signature sequence GYG in both modes I and II), consistent with the required precise operation (selective conduction) of the filter which should not be disrupted by the global rearrangements that modulate the channel gating. The atomic structure and interactions at the selectivity filter are indeed highly specific and selective, and cannot be described by the coarse-grained approach presently adopted. Several detailed simulations by other groups have indeed provided valuable insights on the dynamics of the selectivity filter at full atomic level in the presence of ions and water molecules [15,17,18,19,21]. Our view is that the global

motions characterized here do not interfere with the subtle operation of the selectivity filter, but regulate the collective rearrangements of the TM helices surrounding the pore region, *to ensure the predisposition of the structure to channel gating* that may be triggered by various mechanisms in different K+ channels.

The present study provides further evidence for the intrinsic ability of proteins to undergo cooperative changes required for their biological function (32,33,51,52, 60-62). The current understanding is that the topology of inter-residue contacts, or the overall architecture, defines their equilibrium dynamics, or the cooperative fluctuations that incur the lowest energy ascent in the neighborhood of the original equilibrium state; and these structure-induced fluctuations are those required for, or facilitating, biological functional mechanisms. The slowest modes unraveled by NMA are nothing else than these lowest ascent pathways away from the global minimum; and due to their collective nature these modes are relatively insensitive to atomic details, hence the utility of coarse-grained models such as GNM. This type of structure-encoded dynamics and allosteric effects are presumably further enhanced by structural symmetry in the case of multimeric enzymes or receptors (60) and the four-fold symmetric potassium channels are probably no exception to this generic behavior of biomolecular systems.

Acknowledgments

We thank Dr. AJ Rader and Dr. D Tobi for useful discussions. Partial support from NIH 1 P20 GM065805-01A1 and NSF ITR Grant EIA-0225636 is gratefully acknowledged.

References

1. Hille,B. 2001. Ion Channels of Excitable Membranes, 3rd Edition, Sinauer, Sunderland, Massachusetts, USA pp 5.

2. Ashcroft, F.M. 2000. Ion Channels and Disease. Academic Press, San Diego pp 472.

3. Doyle, D.A., J.M. Cabral, R.A. Pfuetzner, A. Kuo, J.M. Glubis, S.L. Cohen, B.T. Cahit, and R. MacKinnon. 1998. The structure of the potassium channel: molecular basis of K^+ conduction and selectivity. *Science* 280:69-76.

4. Jiang,Y., A. Lee, J. Chen, M. Cadene, B.T. Chait, and R. MacKinnon. 2002. Crystal structure and mechanism of a calcium-gated potassium channel. *Nature* 417:515-522.

5. Kuo,A., J.M. Gulbis, J.F. Antcliff, T. Rahman, E.D. Lowe, J. Zimmer, J. Cuthbertson, F.M. Ashcroft, T. Ezaki and D. Doyle. 2003. Crystal structure of the potassium channel KirBac1.1 in the closed state. *Science* 300:1922-1926.

6. Jiang, Y., A. Lee, J. Chen, V. Ruta, M. Cadene, B.T. Chait and MacKinnon, R. 2003. X-ray structure of a voltage-dependent K^+ channel. *Nature* 423:33-41.

7. Long, S.B., E.B. Campbell and R. MacKinnon 2005. Crystal Structure of a mammalian voltage-dependent *Shaker* family K^+ channel. *Science* 309:897-903.

8. Berman, H.M., J. Westbrook, Z. Feng, G. Gilliland, T.N. Bhat, H. Weissig, I.N. Shindyalov, P.E. Bourne. 2000. The Protein Data Bank. *Nucleic Acids Research*, 28, 235-242.

9. Enkvetchakul**,** D.**,** I.Jeliazkova**,** and C. G. Nichols 2005. Direct Modulation of Kir Channel Gating by Membrane Phosphatidylinositol 4,5-Bisphosphate *J. Biol. Chem*. 280: 35785-35788.

10. Swartz, K.J. 2004. Opening the gate in potassium channels. *Nat. Struct. Biol.* 11: 499-501.

11. Webster, S.M., Del Camino, D., Dekker, J.P. & Yellen, G. (2004) *Nature* 428:864-868.

12. Papazian, D.M., Schwarz, T.L., Tempel, B.L., Jan, Y.N. & Jan, L.Y. (1987) *Science* 237:749-753.

13. Perozo, E., D.M. Cortes, and L.G. Cuello. 1999. Structural rearrangements underlying K^+ channel activation. *Science* 285:73-78.

14. Perozo, E. 2002. New Structural perspectives on K^+ channel gating. *Structure* 10:1027-1029.

15. Shrivastava, I.H., and M.S.P. Sansom. 2000. Simulations of ion permeation through a K channel: molecular dynamics of KcsA in a phospho-lipid bilayer. *Biophys J*. 78:557-570.

16. Shrivastava, I.H., and M.S.P. Sansom. 2002. Molecular dynamics simulations and KcsA channel gating. *Euro. Biophys J*. 31:207-216.

17. Bernèche, S. and B. Roux. 2000. Molecular dynamics of the KcsA K^+ channel in a bilayer membrane. *Biophys J*. 78:2900-2917.

18. Domene, C., and M.S.P. Sansom. 2003. Potassium Channel, Ions, and Water: Simulation studies based on the High Resolution X-Ray structure of KcsA. *Biophys J*. 85:2787-2800.

19. Allen, T.W., S. Kuyucak, and S.H. Chung. 1999. *Biophys J.* Molecular Dynamics study of the KcsA potassium channel. *Biophys J.* 77:2502-2516.

20. Capener, C.E., I.H. Shrivastava, K.M. Ranatunga, L.R. Forrest, G.R. Smith, and M.S.P. Sansom. 2000. Homology modeling and molecular dynamic simulation studies of an inward rectifier potassium channel. *Biophys J*. 78:2929-2942.

21. Guidone, L., V. Torre, and P. Carloni. 2000. Water and potassium dynamics inside the KcsA K channel. FEBS *Lett* 477:37-42.

22. Roux, B. and K. Schulten. 2004. Computational studies of membrane channels. *Structure* 12:1343-1351.

23. Biggin, P.C. and M.S.P. Sansom. 2002. Open-state models of a potassium channel. *Biophys J*. 83:1867-1876.

24. Tikhonov, D.B., and B.S. Zhorov. 2004. In Silico Activation of KcsA K^+ Channel by Lateral Forces Applied to the C-Termini of Inner Helices. *Biophys J*. 87:1526-1536.

25. Bernèche, S. and B. Roux. 2001. Energetics of Ion Conduction through the K^+ Channel. *Nature* 414:73-77.

26. Sansom, M.S.P., I.H. Shrivastava, J.N. Bright, J. Tate, C.E. Capener, and P.C. Biggin. 2002. Potassium channels: structures, models, simulations. *Biochim Biophys Acta* 1565:294-307.

27. Åqvist, J. and V. Luzhkov. 2000. Ion permeation mechanism of the potassium channel. *Nature* 404:881-884.

28. Brooks, B., and M. Karplus. 1983. Harmonic dynamics of proteins normal-modes and fluctuations in bovine pancreatic trypsin inhibitor. *Proc. Natl. Acad. Sci. USA* 80:6571-6575.

29. Go,N., T. Noguti, and T. Nishikawa. 1983. Dynamics of a small globular protein in terms of low-frequency vibrational modes. *Proc. Natl Acad. Sci. USA* 80:3696–3700.

30. Levitt, M., C. Sander, and P.S. Stern. 1985. Protein normal-mode dynamics: Trypsin inihibitor, crambin, ribonuclease and lysozyme. *J. Mol. Biol*. 181:423-447.

31. Kitao, A. and N. Go. 1999. Investigating protein dynamics in collective coordinate space. *Curr. Opin. Struct. Biol*. 9:164-169.

32. Ma, J. 2005. Usefulness and limitations of normal mode analysis in modeling dynamics of biomolecular complexes. *Structure* 13:373-380.

33. Bahar, I., and A.J. Rader. 2005. Coarse-grained normal mode analysis in structural biology. *Curr Opin Struct Biol.* 15:1-7.

34. Shen, Y., Y. Kong, and J. Ma. 2002. Intrinsic flexibility and gating mechanism of the potassium channel KcsA . *Proc. Natl. Acad. Sci. USA* 99:1949-1953.

35. Tirion, M.M. 1996. Large amplitude elastic motions in proteins from a single-parameter atomic analysis. *Phys. Rev. Lett.* 77:1905-1908.

36. Bahar, I., A.R. Atilgan, and B. Erman. 1997. Direct evaluation of thermal fluctuations in protein using a single parameter harmonic potential. *Folding Des*. 2:173-181.

37. Haliloglu, T., I. Bahar, and B. Erman. 1997. Gaussian dynamics of folded proteins. *Phys. Rev Lett.* 79:3090-3093.

38. Flory, P.J. 1976. Statistical thermodynamics of random networks. *Proc. Royal Soc. A* 351:351-378.

39. Bahar, I., B. Erman, R.L. Jernigan, A.R. Atilgan and D.G. Covell. 1999. Collective motions in HIV-1 reverse transcriptase: examination of flexibility and enzyme functions. *J. Mol. Biol*. 285:1023-1037.

40. Bahar, I. and R.L. Jernigan. 1998. Vibrational dynamics of transfer of RNAs: comparison of the free and synthetase bound forms. *J. Mol. Biol.* 281:871-884.

41. Atilgan, A.R., S.R. Durrell, R.L. Jernigan, M.C. Demirel, O. Keskin, and I. Bahar. 2001. Anisotropy of fluctuation dynamics of proteins with an elastic network mode. *Biophys J*. 80:505-515.

42. Zheng W., B.R. Brooks, S. Doniach, and D. Thirumalai. (2005) Network of dynamically important residues in the open/closed transition in polymerases is strongly conserved. *Structure* 13:565-77.

43. Zheng W., and B. R. Brooks. Identification of dynamical correlations within the myosin motor domain by the normal mode analysis of an elastic network model. *J Mol Biol*.346:745-59.

44. Haider,S., A. Grotessi, B.A. Hall, F.M. Ashcroft, and M.S.P. Sansom. 2005. Conformational dynamics of the Ligand-Binding Domain of Inward Rectifier K Channels as Revealed by Molecular dynamics Simulations: Toward an Understanding of Kir Channel Gating. *Biophys* J. 88:3310-3320.

45. Ming, D., Y. Kong, M.A. Lambert,, Z. Huang, and J. Ma. 2002**.** How to describe protein motion without amino acid sequence and atomic coordinates? *Proc Natl Acad Sci USA* 99: 8620-8625.

46. Zheng, W. and S. Doniach. 2003. A comparative study of motor-protein motions by using a simple elastic-network model. *Proc. Natl. Acad. Sci. USA* 100:13253-13258.

47. Tama, F., M. Valle, J. Frank, and C.L. III Brooks. 2003. Dynamic reorganization of the functionally active ribosome explored by normal mode analysis and cryo-electron microscopy. *Proc Natl Acad Sci USA* 100: 9319-9323.

48. Rader, A.J., D.H. Vlad, and I. Bahar. 2005. Maturation Dynamics of Bacteriophage HK97 Capsid *Structure* 3:413-421.

49. Tama, F., and C.L. III Brooks. 2005. Diversity and Identity of Mechanical Properties of Icosahedral Viral Capsids Studied with Elastic Network Normal Mode Analysis**.** *J. Mol. Biol.* 345:299-314.

50. Kundu, S., J.S. Melton, D.C. Sorensen, and G.N. Jr Phillips. 2002. Dynamics of proteins in crystals: comparison of experiment with simple models. *Biophys J*. 83:723-732.

51. Tama F. and Y.-H. Sanejouand. 2001. Conformational changes of proteins arising from normal mode calculations. *Prot. Eng*. 14:1-6.

52. Xu, C., D. Tobi, and I. Bahar. 2003. Allosteric Changes in Protein Structure Computed by a Simple Mechanical Model: Hemoglobin T --> R2 Transition. *J. Mol. Biol.* 333:153-168.

53. Lindhal, E., Hess, B. and Spoel, van der D. 2001. Gromacs 3.0: a package for molecular simulation and trajectory analysis. *J. Mol. Model.* 7:306-317.

54. Zhou, Y., J. H. Morais-Cabral, A. Kaufman, and R. Mackinnon, R. (2001) Chemistry of Ion Coordination and Hydration Revealed by a K+ Channel-Fab Complex at 2.0 Å Resolution *Nature* 414: 43-.

55. Irizarry, S.N., E. Kutluay, G. Drews, S.J. Hart and L. Heginbotham. 2002. Opening the KcsA K^+ channel: tryptophan scanning and complementation analysis lead to mutants with altered gating. *Biochem*istry. 41:13653-13662.

56. Yifrach, O. and MacKinnon, R. 2002. Energetics of pore opening in a voltage-gated K^+ channel. *Cell* 111:231-239.

57. Lu, Z., Klem, A.M. and Ramu, Y. 2001. Ion conduction pore is conserved among potassium channels. *Nature* 413:809-813.

58. Holmgren, M., Shin, K.S. and Yellen, G. 1998. The activation gate of a voltage-gated K^+ channel can be trapped in the open state by an inter-subunit metal bridge. *Neuron* 21:67-621.

59. del Camino, D., Yellen, G. 2000. Blocker protection in the pore of a voltage-gated K^+ channel an its structural implications. *Nature* 403:321-325.

60. Changeux, J.-P., and S.J. Edelstein. 2005. Allosteric mechanisms of signal transduction. *Science*. 308:1424-1428.

61. Tobi, D. and Bahar,I. 2005. Structural changes involved in protein binding correlate with intrinsic motions of proteins in the unbound state. *Proc. Natl. Acad. Sci. USA* 102:18908-18913.

62. Eisenmesser, E.Z., Millet, O.,Labeikovsky, W., Korzhnev, D.M., Wolf-Watz, M., Bosco, D.A., Skalicky, J.J., Kay, L.E. and Kern, D. (2005) Intrinsic dynamics of an enzyme underlies catalysis, *Nature* ***438***, 117-121

63. Thompson, J.D., D.G. Higgins and T.J. Gibson. 1994. ClustalW: improving the sensitiviy of progressive multiple sequence alignment through sequence weighting, positions-specific gap penalties and weight matrix choice. *Nuc. Acids Res.* 22:4673-4680.

64. Kraulis, P.J. 1991.MOLSCRIPT: a program to produce both detailed and schematic plots of protein structures. *J. Appl. Crystallogr*. 24:946-950.

65. Smart, O.S., J.M. Goodfellow, and B.A. Wallace. 1993. The pore dimensions of gramicidin. *Biophys J.* 65:2455-2460.

Table 1. Potassium channels structurally characterized to date.

Protein	(Ref)	PDB† ID	Organism	Resolution(Å)	N‡	GYG¶
KcsA*	(54)	1k4c	*Streptomyces lividans*	2.0	103	77-79
MthK	(4)	1lnq	*Methanobacterium thermoautotrophicum*	3.3	80	61-63
KirBac	(5)	1p7b	*Burkholderia pseudomallei*	3.5	94	112-114
KvAP	(6)	1orq	*Aeropyrum pernix*	3.2	106	198-200
Shaker	(7)	2A79	*Rattus norvegicus*	2.9	109	376-378

*The coordinates of KcsA in the high resolution K+channel/Fab complex determined by Zhou et al (54) is considered in the present study; † The Protein Data Bank (8); ‡Number of residues refers to those in the pore-forming regions of the monomers, which have been included in the computations; ¶Residue numbers corresponding to the signature sequence (GYG) in each PDB file.

Figure Legends

Figure 1. **Sequence and structure of the pore region of five structurally known potassium channels.** (a) Alignment of the pore region sequences. See Table 1 for the nomenclature and source. The regions corresponding to the helices TM1 and TM2 and the P-loop are indicated by yellow, green and red arrows, respectively. The alignment was performed using ClustalW (63) Fully or highly conserved regions are shown in black, moderately conserved in gray. Two regions of interest are the signature motif GYG at the selectivity filter, and the conserved G on TM2, both enclosed in magenta boxes (see also Figure 2a) (b) Structural comparison of the pore forming regions of the K^+ channels aligned in panel a. These are all tetrameric structures, the monomers of which contain either 2 TM helices (KcsA, MthK and KirBac) colored yellow (TM1) and green (TM2), or 6 TM helices (KvAP and Shaker) denoted as S1-S6. Only the pore forming helices S5 and S6, equivalent to TM1 and TM2, are displayed here, along with the P-helix/loops region, colored red.

Figure 2. **Structure and dynamics of KcsA**. (a) Ribbon diagram of the KcsA, based on the PDB structure deposited by Doyle et al (3). Each monomer contains two TM helices, TM1 (outer; yellow) and TM2 (inner; green). The flow of K^+ ions across the selectivity filter based on MD simulations (15) is schematically shown. Other regions of functional importance are the gate near the intracellular region and the turret at the extracellular surface. The short black arrows indicate the movements suggested by spin labeling experiments (13) for gate opening. The figure was made using Molscript (64). (b) Equilibrium fluctuations as a function of residue index. Left and right ordinates refer to the B-factors and mean-square fluctuations respectively of individual residues, which are related as $B_i = 8\pi^2\langle(\Delta R_i)^2\rangle/3$ where i is the residue index (abscissa). The three curves describe the results obtained from GNM analysis (red), MD simulations (black) and X-ray crystallography (blue). The correlation coefficient between experimental data and theoretical results are 0.93 (GNM) and 0.85 (MD), and that between the two theoretical results is 0.95.

Figure 3. Residue mobilities induced by two dominant mechanisms of global motion. The panels describe the square-displacements of residues driven by the two most cooperative (lowest frequency) motions predicted by the GNM, referred to as global motions of type I and II, for all five structures (see Figure 1b) examined. The left panels display the results for motion I, for the entire tetramer. This motion results from the combination of two degenerate modes that activate each the diagonally positioned pairs of monomers (see Figure 3). The right panels display the mobilities induced by for both modes I (black) and II (red). Results are displayed for monomers only, as they are repeated across all four monomers.

Minima indicated by blue 'x' and red '●' symbols on the abscissa coincide with the signature sequence GYG, and the conserved Gly residues on the TM2 helices, respectively (Fig 1a). Those indicated by '▲' on the right refer to small hydrophobic residues at central positions on TM1 helices, which closely interact with the conserved Gly on TM2 helices. These three sets define the key sites that act as hinges/anchors in coordinating the two global mechanisms.

Figure 4. Mobilities in global modes shown by color-coded diagrams for KcsA, KirBac and Shaker. The slowest global mode (mode type I) is two fold degenerate. The corresponding ribbon diagrams are shown on the left and middle columns. The second lowest frequency mode (mode type II) is illustrated in the right column. Color code is red-orange-green-cyan-blue in the order of decreasing mobility. Note that mode type I involves the pairwise motions of oppositely positioned monomers, while mode type II is cylindrically symmetric.

Figure 5. Master curves for global dynamics of potassium channels. (a) Superposition of the most cooperative global mode shape (type I) for KcsA (red), KirBac (green), KvAP (blue) ,Shaker (magenta) and MthK (black), plotted for one monomer. The abscissa refers to the residue indices of MthK. Inset shows a ribbon diagram of KcsA, with two monomers removed for clarity, highlighting the selectivity filter residues GYG, in space filling representation. (b) Superposition of the global mode shape (type II) for the same set of proteins. The abscissa refers to the residue indices of MthK. Inset shows a ribbon diagram of KcsA, with two subunits removed for clarity, highlighting the conserved glycine on TM2 in space filling representation.

Figure 6. Dynamic equilibrium between fluctuating conformations. Ribbon diagrams represent different deformed models for KcsA (panel a and b) and Shaker (panel c), generated using eq 6 for mode types I and II. a: Side view of deformed model for type I mode for s_I = -75 (top) and s_I = -100 (bottom). b: Top view of deformed models for mode type I obtained using s_I = -75 (top right), s_I = +75 (bottom left), and for mode type II, s_{II} = -100 (top left), s_{II} = 100 (bottom right). The figure in the middle is that of the crystal structure. c. Counterpart of panel b for Shaker.

Figure 7. Panel a: Pore-radius profiles as a function of the position along the cylindrical (Z-) axis. A. The radii are computed for the crystal structure (black) and the deformed conformations at s_{II} = -200 (red, solid) and s_{II} = +200 (red, dashed). Panel b: shows solid-sphere representation of the inner surface of the channel at the pore region for the crystal structure (left), for the model of the open form (right) at s_{II} = -200 with the corresponding backbone structures superimposed onto the pore-surface. The color code for the solid-sphere representation is: red, pore radius < 1.15 Å; green, 1.15 Å < radius < 2.30 Å; and blue, radius > 2.30 Å. The pore radius profiles were generated using HOLE (65). In the inset of panel a

is the backbone of the crystal structure (blue) superimposed onto the model of the open form (red). Two monomers have been deleted for clarity.

Figure 8. Cartoon representation of the TM2 helices of the deformed models of KcsA, KirBac and Shaker, at different values of scaling parameter (eq 6). Panel a: Top row: Cartoon representation of closed and open models for KcsA, proposed as a model for molecular mechanism of gating, based on experimental data (Fig. 7 in ref 13). Middle row: TM2 helices in the original structure (s_{II} = 0) and in the conformation induced by mode II (s_{II} = -100) for KcsA. Bottom row: TM2 helices of Shaker in the PDB structure (s_{II} = 0) and the predicted structure deformed along mode II (s_{II} = -55). Panel b: Top row: Cartoon representation of KcsA (red) and MthK (green) TM structures, illustrating the model proposed by Perozo and coworkers for a 'hinge-gating' mechanism at the intracellular gate (Fig. 1 in ref 14). Middle row: KcsA TM2 helices at s_{II} = -150, top view (left) and side view (right). Highlighted residue at the kink is T^{107}. Bottom row: KirBac TM2 helices at s_{II} = -73, top view (left) and side view (right). Conserved glycine (G^{134}) emerging as kink residue is highlighted.

Supplementary material

Movie 1: KcsA_torsion_top.mpg
A movie of the motions observed in slow mode type II, for KcsA, as viewed from the extracellular end.

Movie 2: KcsA_torsion_side.mpg
A movie of the motions observed in slow mode type II , for KcsA, as viewed from the side perpendicular to the channel pore axis.

Movie 3: Shaker_torsion_top.mpg
A movie of the motions observed in slow mode type II, Shaker, as viewed from the extracellular end.

Movie 4: Shaker_torsion_side.mpg
A movie of the motions observed in slow mode type II, Shaker, as viewed from side perpendicular to the channel pore axis.

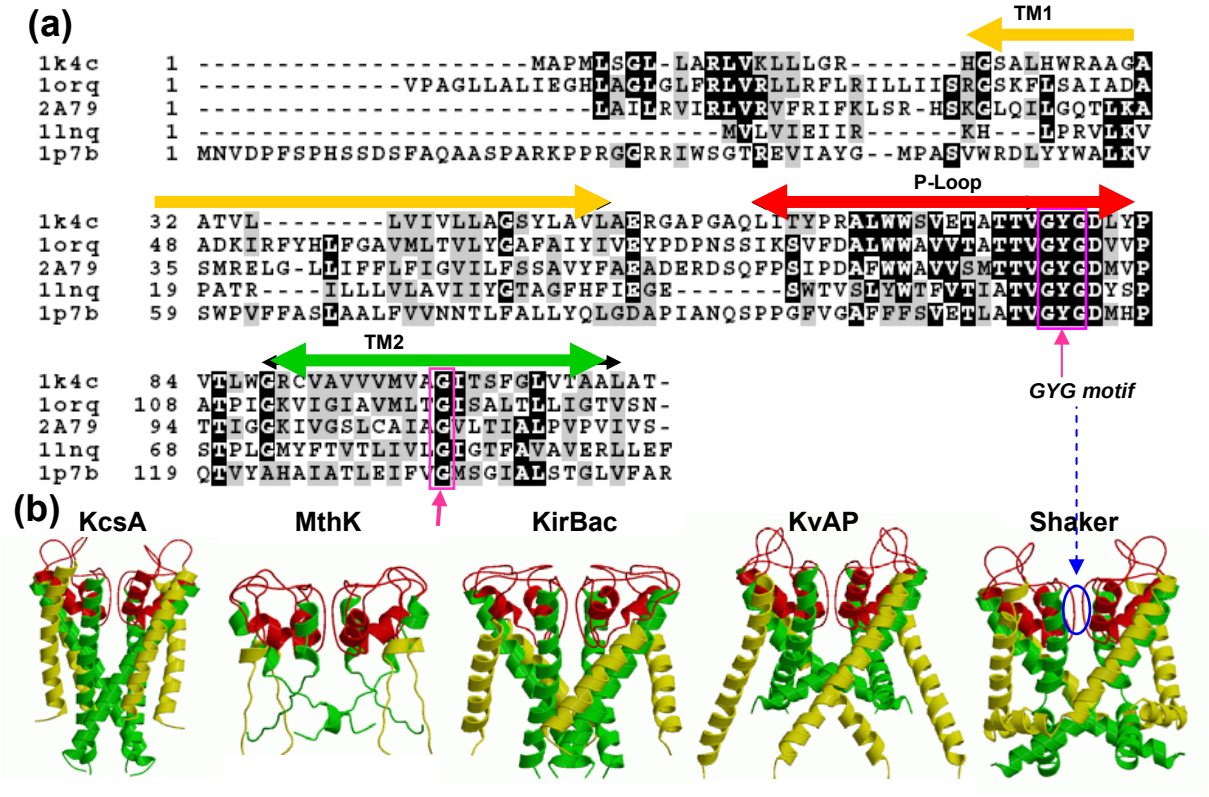
(a)
TM1
P-Loop
TM2
GYG motif
1k4c 1 ----------MAPMLSGL-LARLVKLLLGR-------HGSALHWRAAGA
1orq 1 ----------VPAGLLALIEGHLAGLGLFRLVRLLRFLRILLIISRGSKFLSAIADA
2A79 1 ----------LAILRVIRLVRVFRIFKLSR-HSKGLQILGQTLKA
1lnq 1 ----------MVLVIEIIR------KH---LPRVLKV
1p7b 1 MNVDPFSPHSSDSFAQAASPARKPPRGGRRIWSGTREVIAYG--MPASVWRDLYYWALKV
1k4c 32 ATVL--------LVIVLLAGSYLAVLAERGAPGAQLITYPRALWWSVETATTVGYGDLYP
1orq 48 ADKIRFYHLFGAVMLTVLYGAFAIYIVEYPDPNSSIKSVFDALWWAVVTATTVGYGDVVP
2A79 35 SMRELG-LLIFFLFIGVILFSSAVYFAEADERDSQFPSIPDAFWWAVVSMTTVGYGDMVP
1lnq 19 PATR----ILLLVLAVIIYGTAGFHFIEGE-------SWTVSLYWTFVTIATVGYGDYSP
1p7b 59 SWPVFFASLAALFVVNNTLFALLYQLGDAPIANQSPPGFVGAFFFSVETLATVGYGDMHP
1k4c 84 VTLWGRCVAVVVMVAGITSFGLVTAALAT-
1orq 108 ATPIGKVIGIAVMLTGISALTLLIGTVSN-
2A79 94 TTIGGKIVGSLCAIAGVLTIALPVPVIVS-
1lnq 68 STPLGMYFTVTLIVLGIGTFAVAVERLLEF
1p7b 119 QTVYAHAIATLEIFVGMSGIALSTGLVFAR
(b)
KcsA
MthK
KirBac
KvAP
Shaker

Figure 1

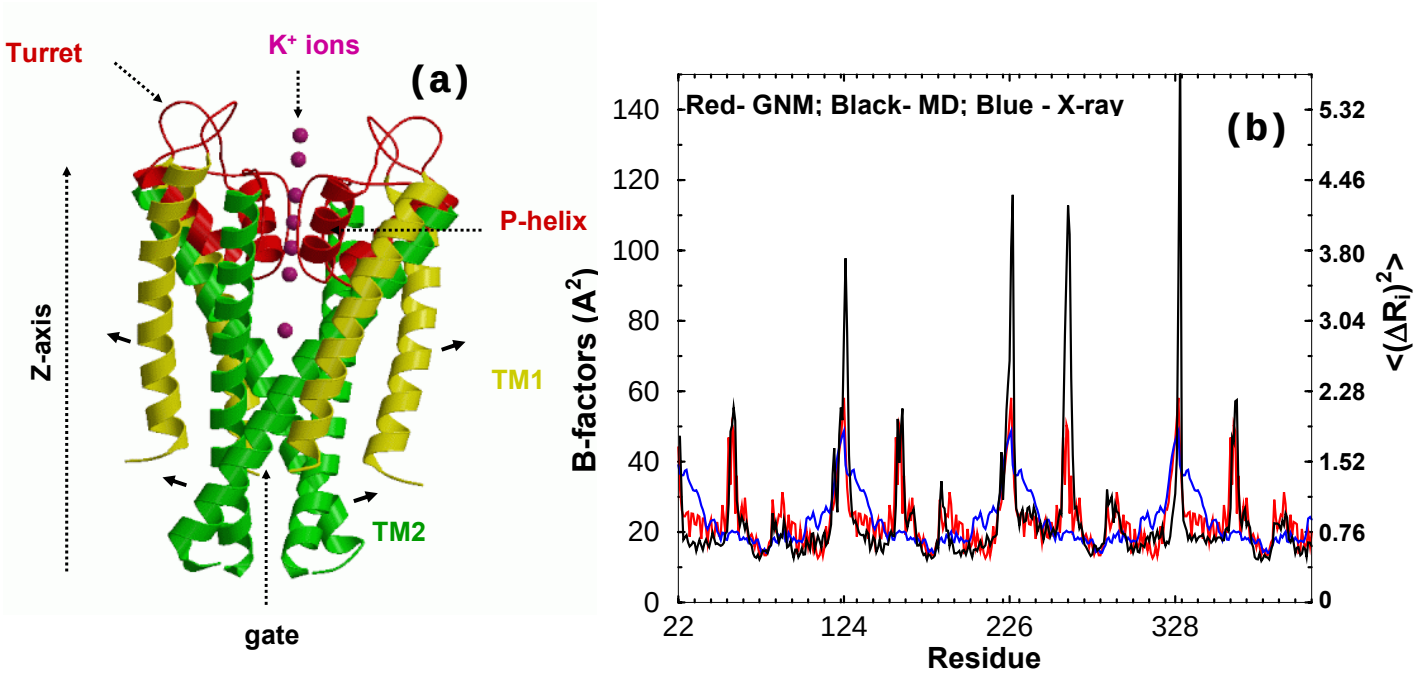
Turret
K+ ions
(a)
P-helix
Z-axis
TM1
TM2
gate
Red- GNM; Black- MD; Blue - X-ray
(b)
B-factors (A2)
<(ΔRi)2>
Residue
0
20
40
60
80
100
120
140
0.76
1.52
2.28
3.04
3.80
4.46
5.32
22
124
226
328

Figure 2

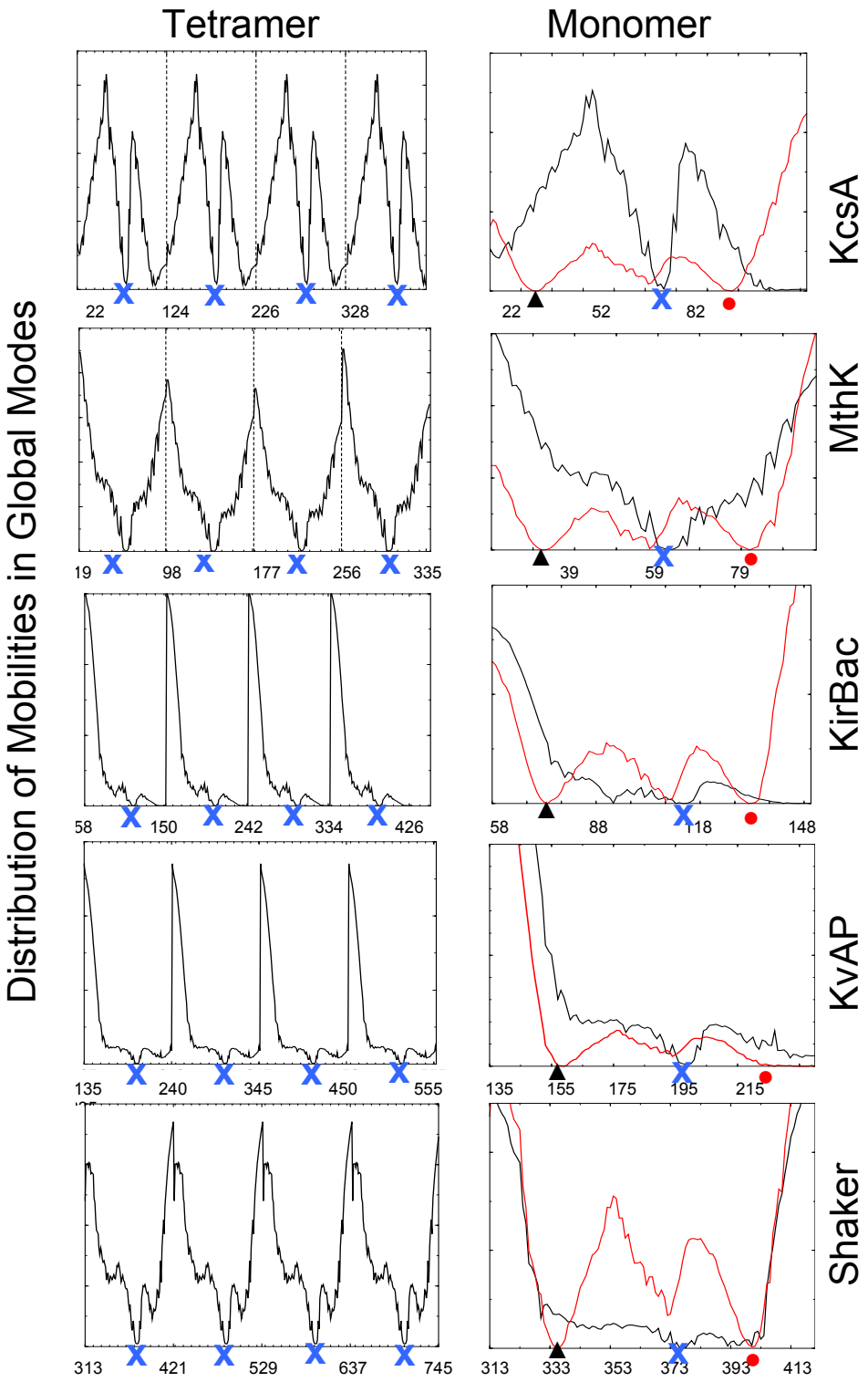
Tetramer
Monomer
Distribution of Mobilities in Global Modes
KcsA
MthK
KirBac
KvAP
Shaker
22 124 226 328
22 52 82
19 98 177 256 335
39 59 79
58 150 242 334 426
58 88 118 148
135 240 345 450 555
135 155 175 195 215
313 421 529 637 745
313 333 353 373 393 413

Figure 3

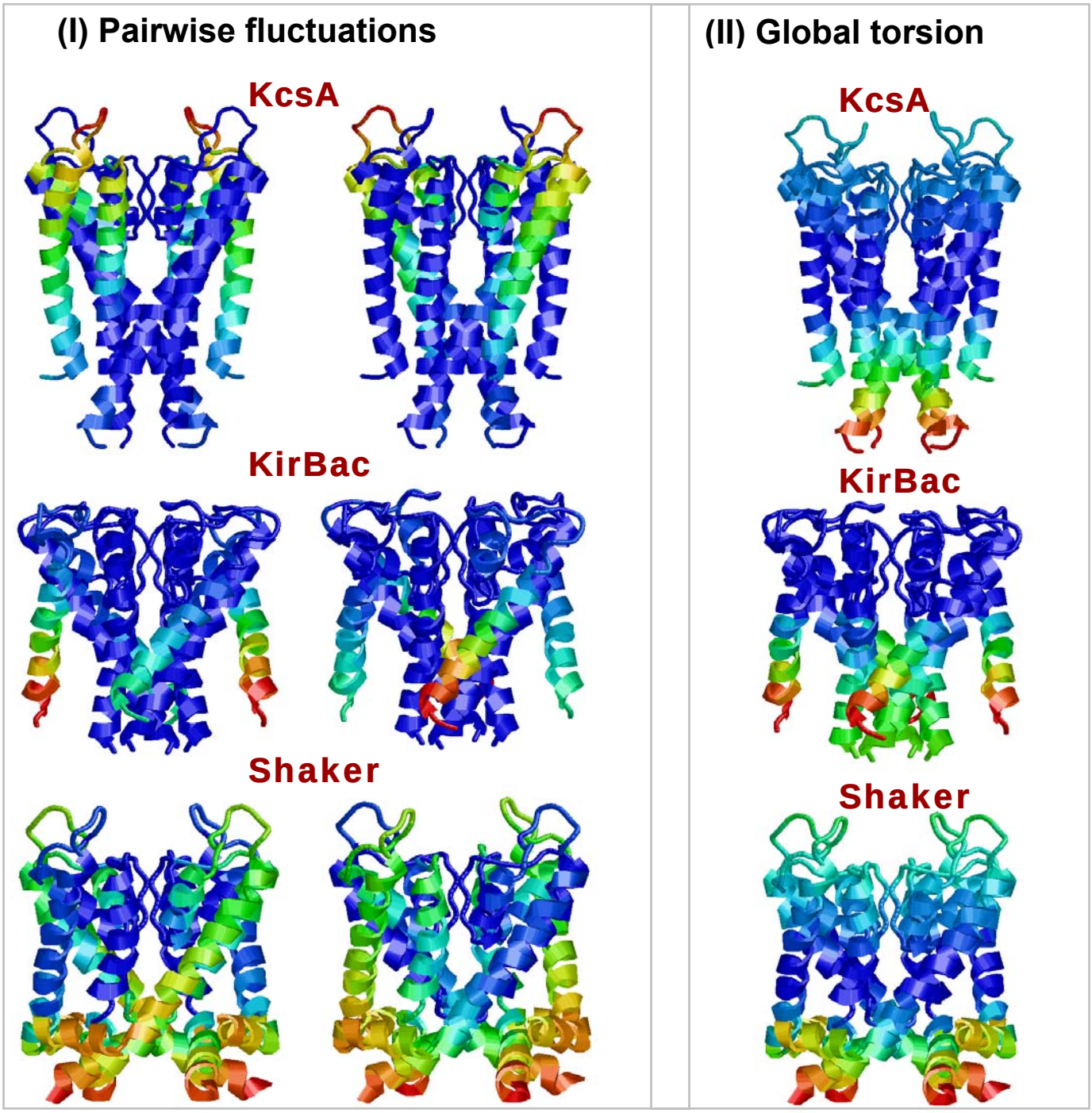
(I) Pairwise fluctuations
KcsA
KirBac
Shaker
(II) Global torsion
KcsA
KirBac
Shaker

Figure 4

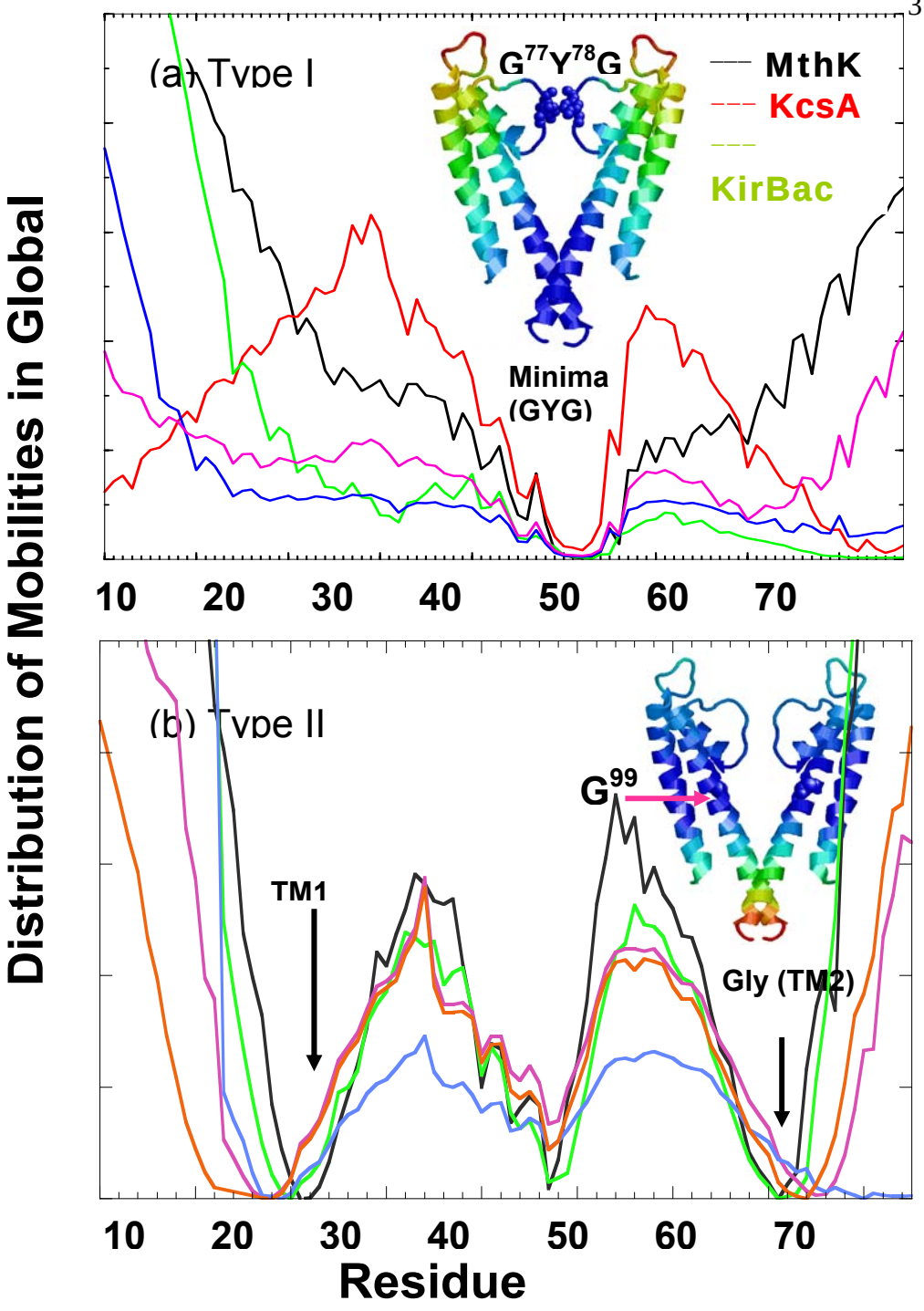
(a) Type I
G77Y78G
MthK
KcsA
KirBac
Minima
(GYG)
10
20
30
40
50
60
70
(b) Type II
G99
TM1
Gly (TM2)
10
20
30
40
50
60
70
Residue
Distribution of Mobilities in Global

Figure 5

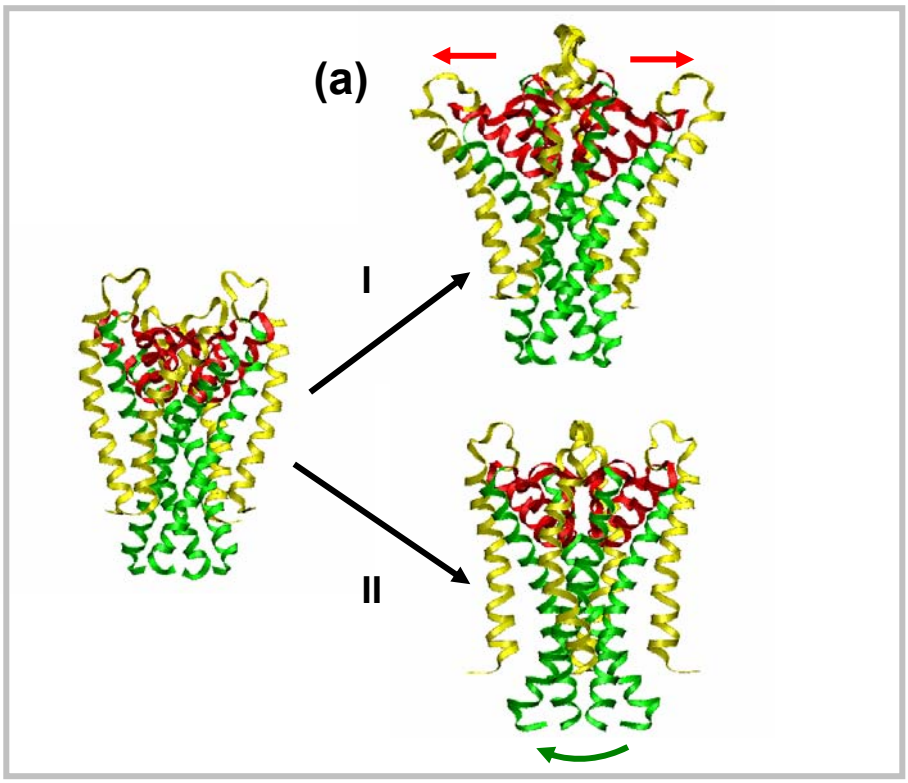
(a)
I
II

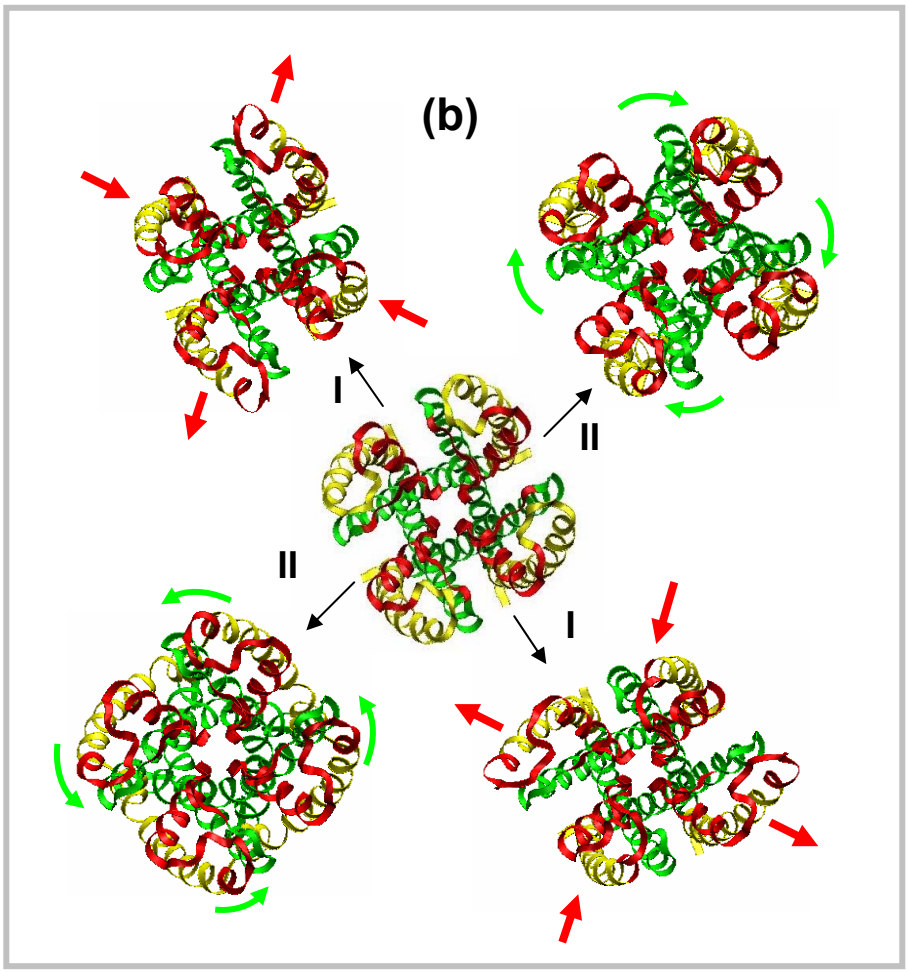
(b)
I
II
II
I

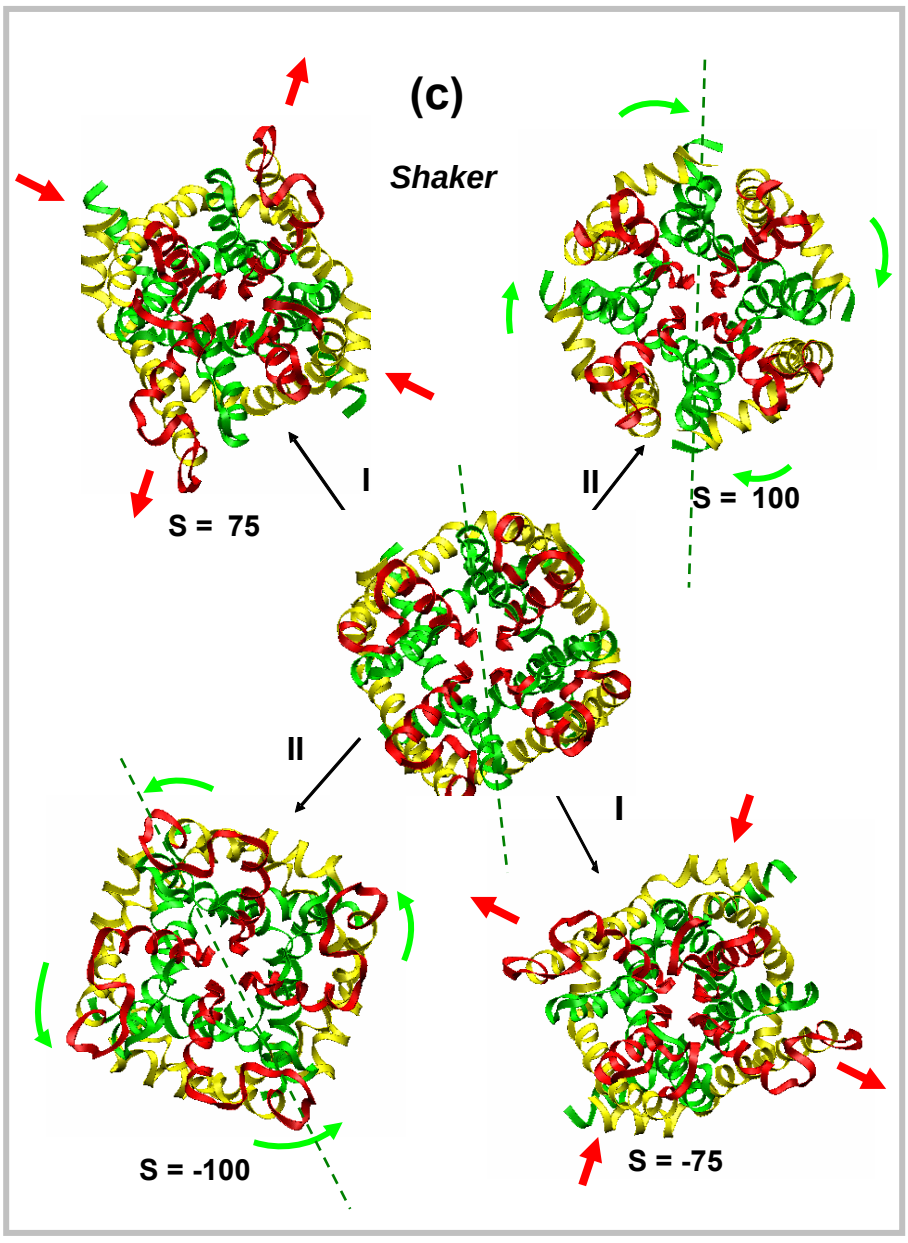

Figure 6

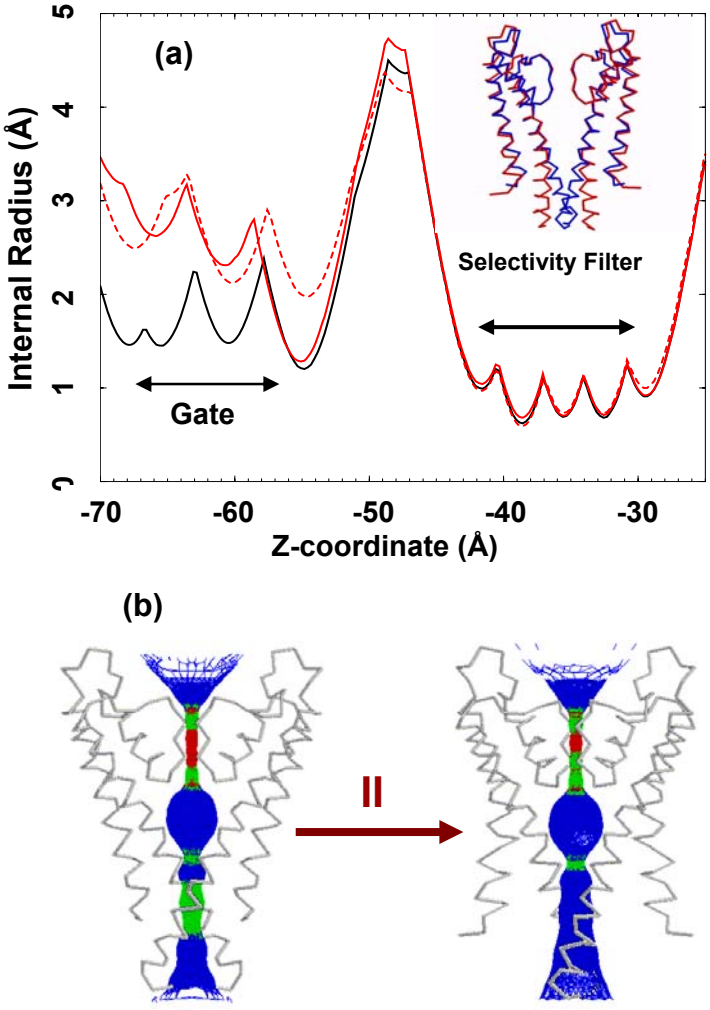
(a)
Internal Radius (Å)
Selectivity Filter
Gate
Z-coordinate (Å)
(b)

Figure 7

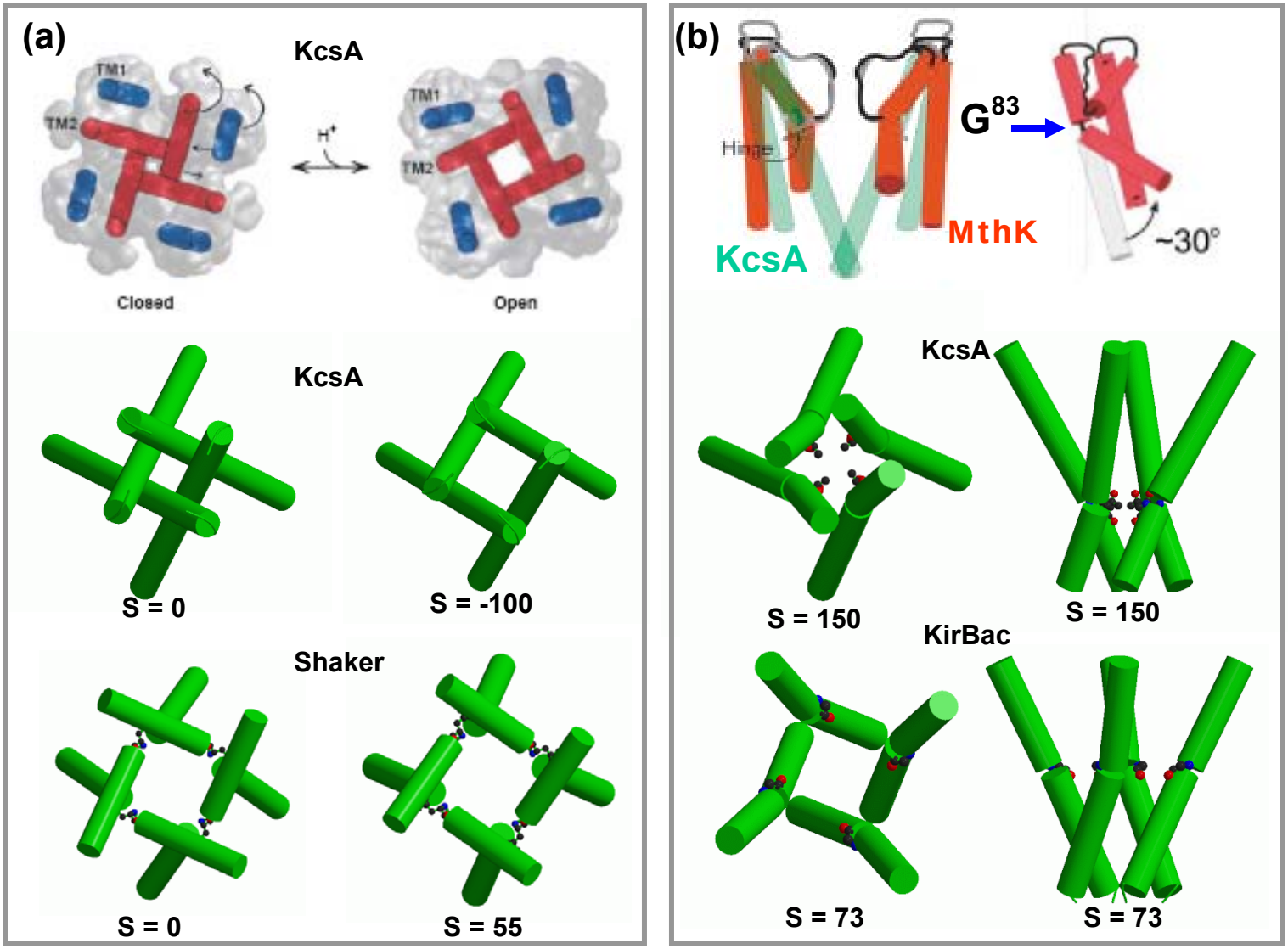
(a)
KcsA
TM1
TM2
H+
TM1
TM2
Closed
Open
KcsA
S = 0
S = -100
Shaker
S = 0
S = 55
(b)
Hinge
G83
MthK
KcsA
~30°
KcsA
S = 150
S = 150
KirBac
S = 73
S = 73

Figure 8